Journal of Materials Science: Materials in Electronics (2019) 30:19108–19118
https://doi.org/10.1007/s10854-019-02266-0

Coupling Bi_2MoO_6 with persulfate for photocatalytic oxidation of tetracycline hydrochloride under visible light

Qinqin Feng[1,2] · Jiabin Zhou[1,2] · Ying Zhang[1]

Received: 5 July 2019 / Accepted: 23 September 2019 / Published online: 10 October 2019

Abstract
In this study, Bi_2MoO_6 nanosheets were fabricated by a facile hydrothermal method. The physicochemical properties and morphology of the as-prepared Bi_2MoO_6 nanosheets were characterized by XRD, XPS, DRS and FESEM technologies. Photocatalytic results indicated that the Vis/Bi_2MoO_6/PS system was much more efficient than Vis/Bi_2MoO_6 and Vis/PS individual binary systems in TC-HCl degradation. The effects of catalyst dosage (0–0.8 g/L), initial TC-HCl concentration (20–120 ppm), PS concentration (0–10 g/L), initial solution pH (2–10) and coexisting anions (Cl^-, NO_3^-, SO_4^{2-}) on the TC-HCl removal efficiency were studied. Recycle experiments proved that the catalyst exhibited excellent stability and reusability in degrading TC-HCl molecules through activation of PS. In addition, trapping experiments revealed that $SO_4^{\cdot-}$ and h^+ were the dominant radicals during degradation process. Finally, the possible mechanism for degrading TC-HCl in the Vis/Bi_2MoO_6/PS system was proposed.

1 Introduction

The discharge of tetracycline hydrochloride (TC-HCl) and other antibiotics into the aquatic environment has been widely recognized as a severe environmental problem [1–3]. The presence of antibiotics in water body could lead to long-term adverse impacts on ecosystems and human health [2, 4, 5]. Much attention has been paid to develop efficient methods such as adsorption [6, 7], electrolysis [8], advanced oxidation processes [9–11] and microbial degradation [12] to degrade the recalcitrant antibiotics. Advanced oxidation processes (AOPs) have been recognized as promising techniques for completely removing tetracycline hydrochloride from polluted water comparing to other wastewater treatments [13, 14].

Among different AOPs, photocatalysis has received much attention as a kind of energy saving and green technology [8, 15, 16]. Bismuth based semiconductors such as Bi_2O_3 [17, 18], Bi_2MoO_6 [19], Bi_2WO_6 [20], $BiVO_4$ [21], Bi_2GeO_5 [22] and BiOX (X = Cl, Br, I) [23–25] are widely used in photocatalysis for removing toxic organic compounds. As a representative Bi-based photocatalyst, Bi_2MoO_6 could be excited by visible light because of its suitable band gap (2.4–2.8 eV) [26]. Moreover, its unique crystal structure is composed of altering $(Bi_2O_2)^{2+}$ and $(MoO_6)^{2-}$ layers, which was proved to be beneficial to charge transfer [27]. However, it is still hard for Bi_2MoO_6 to meet the standard of practical applications due to the fierce recombination rate of photo-excited electron–hole pairs. Up to now, several methods such as controllable synthesis [28], ion doping [29], self-doping [30] and constructing heterojunction [31] have been developed to promote the photocatalytic efficiency of Bi_2MoO_6.

In recent years, coupling of photocatalysis and electron acceptors has been proved to be an effective method to produce a rate-enhancing effect on degrading pollutants [32]. Compared to H_2O_2, persulfate (PS) is easier to be transported, applied and stored due to its solid state at room temperature [33, 34]. After trapping the electrons on the conduction band, PS is excited with the generation of highly efficient sulfate radical ($SO_4^{\cdot-}$) and hydroxyl radical (·OH). Compared to nonselective ·OH, $SO_4^{\cdot-}$ is more selective toward organic pollutants. Moreover, $SO_4^{\cdot-}$ has stronger oxidize activity than ·OH since the redox potential of $SO_4^{\cdot-}$ (2.5–3.1 V) is higher than that of ·OH (1.89–2.72 V) [35]. More recently, integrating photocatalyst, visible light

✉ Jiabin Zhou
jbzhou@swpu.edu.cn

1 School of Resources and Environmental Engineering, Wuhan University of Technology, Wuhan 430070, People's Republic of China

2 College of Chemistry and Chemical Engineering, Southwest Petroleum University, Chengdu 610500, People's Republic of China

and PS to degrade contaminants has attracted more and more interest from researchers [36–38]. However, to the best of our knowledge, the report focused on investigating the photocatalytic process of Bi_2MoO_6 with the assistant of PS is still limited.

Based on the previous studies, the object of our article was to investigate the potential application of Vis/Bi_2MoO_6/PS system in the degradation of TC-HCl. The effects of several important parameters on the removal process of TC-HCl were studied. A possible photocatalytic mechanism was proposed according to free radical scavenging experiments. This study provided a promising way to improve the photocatalytic performance of Bi_2MoO_6 by adding PS.

2 Experimental

2.1 Chemicals

All the reagents were used as-received directly without further purification. Tetracycline Hydrochloride (TC-HCl) was bought from Macklin Biochemical Technology Co., Ltd. (Shanghai, China). All other reagents (bismuth nitrate pentahydrate ($Bi(NO_3)_3{\cdot}5H_2O$), sodium molybdate dihydrate ($Na_2MoO_4{\cdot}2H_2O$), sodium persulfate ($Na_2S_2O_8$), sodium hydroxide (NaOH), nitric acid (HNO_3), absolute ethanol (C_2H_5OH), sodium chloride (NaCl), sodium sulfate (Na_2SO_4), potassium nitrate (KNO_3), tertbutanol (TBA), phenol, ethylenediamine tetraacetic acid disodium salt (EDTA-2Na)) were obtained from Kelong Chemical Reagent Co., Ltd. (Chengdu, China) at analytical grade. Ultrapure water (18.25 MΩ cm at 25 °C) obtained from a Milli-Q system was used throughout experiments.

2.2 Synthesis of Bi_2MoO_6

Bi_2MoO_6 was prepared by a simple hydrothermal method according to the previous articles [39, 40]. At first, 2 mmol (0.97 g) $Bi(NO_3)_3{\cdot}5H_2O$ and 1 mmol (0.24 g) $Na_2MoO_4{\cdot}2H_2O$ were added into 80 mL ultrapure water. Subsequently, the mixture was vigorously stirred at room temperature for 30 min to form homogenous suspension. Then the resultant suspension was transferred to a 100 mL autoclave Teflon vessel and hydrothermally treated at 120 °C for 24 h. After the autoclave cooling down to room temperature naturally, the as-prepared powders were washed with ultrapure water and absolute ethanol for three times in turn and dried at 60 °C for 12 h.

2.3 Characterization of Bi_2MoO_6

The crystal characteristics of the as-prepared Bi_2MoO_6 were measured by powder X-ray diffraction (XRD, RU-200B/D/MAX-RB, Japan) with Cu Kα radiation over the two-theta region of 10°–60°. The surface element compositions were investigated using the X-ray photoelectron spectroscopy (XPS, ESCALAB 250Xi, USA) where C 1s located at 284.6 eV was used as reference standard. The morphological features of Bi_2MoO_6 were recorded on a field emission scanning electron microscopy (FESEM, Regulus8100, Japan). The UV–Vis absorption spectra and diffuse reflectance spectra (DRS) were analyzed by UV–Vis spectrophotometer (Lambda 750S, USA) using $BaSO_4$ as reference standard.

2.4 Degradation experiments and analyses

The photocatalytic activities of Bi_2MoO_6 were evaluated by degrading TC-HCl under visible light irradiation. A 300 W Xe lamp (CEL-HXF300/CEL-HXUV-300) equipped with a 420 nm cut-off filter was used as a light source. The solution pH was not adjusted unless specially illustrated. A desired amount of Bi_2MoO_6 was introduced to 100 mL TC-HCl solution at first. The obtained mixture was vigorously stirred in the dark for 30 min to establish the adsorption/desorption equilibrium. After stirring, a certain amount of PS and other additives if necessary were added. Subsequently, the suspension was exposed to visible light to initiate the reaction. At designated time interval, 3 mL sample was extracted and centrifuged immediately to remove the catalyst. The residual concentration of TC-HCl was determined by measuring the absorbance at the maximum wavelength of 357 nm on a UV–Vis spectrophotometer (UVmini-1280, Shimadzu).

The degradation ratio (DR) was calculated via the following equation:

$$DR(\%) = (1 - C/C_0) \times 100\% \quad (1)$$

where C_0 is the initial concentration of TC-HCl at time 0, C represents the concentration of TC-HCl at a given period of time t.

The pseudo-first-order kinetic model was used to investigate the degradation performance of TC-HCl under different systems. The value of apparent kinetic constant (K_{app}) was calculated according to the following formula [41]:

$$-\ln(C/C_0) = K_{app}t \quad (2)$$

3 Results and discussion

3.1 Characterization of Bi_2MoO_6

The X-ray diffraction pattern of the as-prepared Bi_2MoO_6 was shown in Fig. 1. Well-defined peaks at 10.86°, 23.52°, 28.26°, 32.54°, 33.06°, 36.04°, 46.78°, 47.16°, 55.56°, 56.22°, 58.56° were respectively responding to the (020), (111), (131), (200), (060), (151), (202), (260), (331), (280), (262) planes of orthorhombic Bi_2MoO_6 phase (JCPDS card

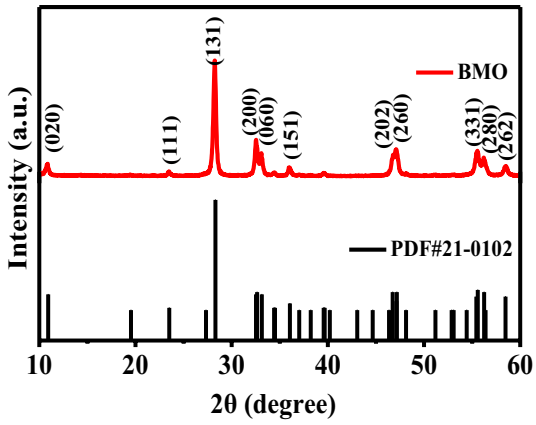

Fig. 1 XRD pattern of the as-prepared Bi_2MoO_6 photocatalyst

no. 21-0102) [40]. No other obvious peaks could be found, indicating the high purity of Bi_2MoO_6.

XPS analysis was carried out to investigate the chemical compositions and states of surface elements. As shown in Fig. 2a, signals of Bi, Mo, O and C were found in the survey spectrum of Bi_2MoO_6, where C came from the XPS instrument. The Bi 4f core-level spectra demonstrated a binding energy at 164.3 eV for Bi $4f_{5/2}$ and at 159.0 eV for Bi $4f_{7/2}$, revealing that Bi was in trivalent oxidation state [42]. For the spectrum in the Mo 3d region, two sharp peaks located at 235.4 eV and 232.3 eV were respectively ascribed to the Mo $3d_{3/2}$ and Mo $3d_{5/2}$, which corresponded to the + 6 oxidation state of Mo [43]. The detailed O 1 s spectra was shown in Fig. 2d. The peak at 529.9 eV could be assigned to the lattice oxygen [44].

The microstructure and morphology of Bi_2MoO_6 were characterized by FESEM technique. Figure 3 presented the representative FESEM images of Bi_2MoO_6. It was clearly that Bi_2MoO_6 was composed of many irregular nanosheets with smooth surface. With respect to the high-resolution image (Fig. 3b), the nanosheets were quite thin and its width ranged from 500 nm to 2 μm. Moreover, the nanosheets were stacked closely.

The UV–Vis DRS in the range of 200–800 nm was utilized to determine the optical properties of Bi_2MoO_6. As shown in Fig. 4a, it was obvious that the photocatalyst had a strong absorption capacity in visible light region. The corresponding band gap energy (E_g) of Bi_2MoO_6 could be

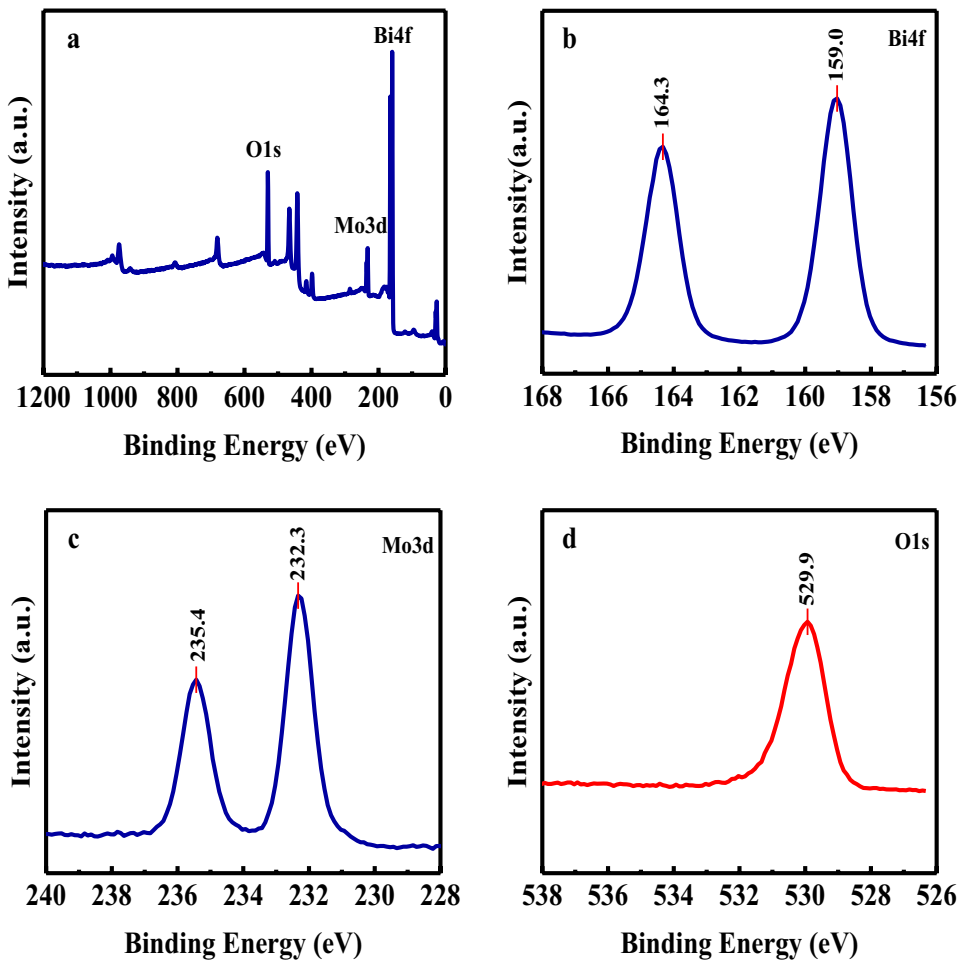

Fig. 2 XPS of Bi_2MoO_6: **a** full spectra of sample; **b** Bi 4f peaks; **c** Mo 3d peaks; **d** O1s peaks

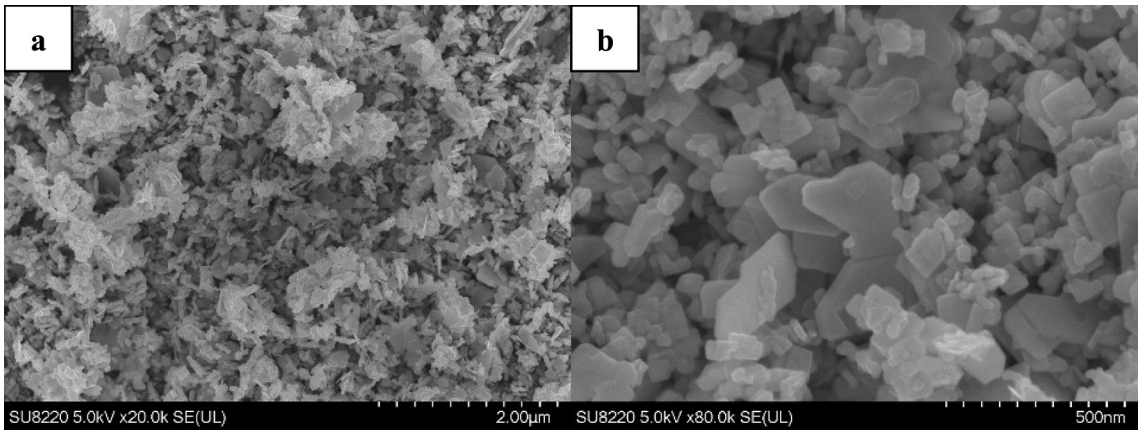

Fig. 3 FESEM images of Bi_2MoO_6

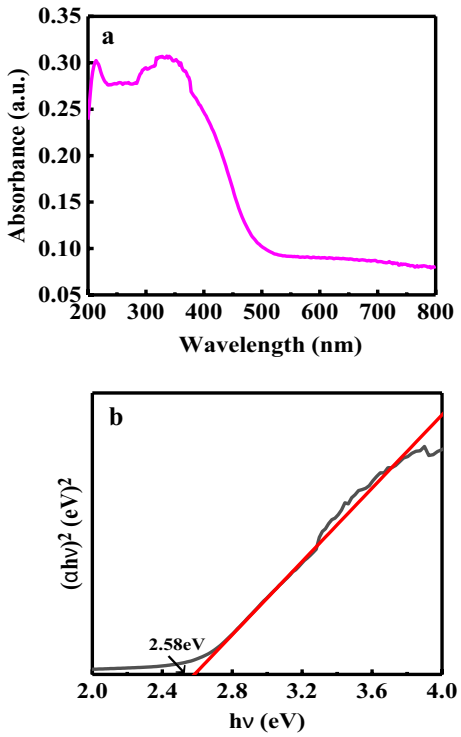

Fig. 4 **a** UV–Vis DRS spectra of Bi_2MoO_6, **b** $(\alpha h\nu)^2$ versus photon energy ($h\nu$) of Bi_2MoO_6

calculated using the following Kubelka–Munk equation [45]:

$$\alpha h\nu = A(h\nu - E_g)^{n/2} \tag{3}$$

where α, h, ν, A are the absorption coefficient, Planck constant, light frequency and the proportionality constant, respectively. The value of n depending on transition nature is 1 due to the direct band-gap characteristic of Bi_2MoO_6 [45]. Therefore, the equation can be expressed as another form as follows:

$$(\alpha h\nu/A)^2 = h\nu - E_g \tag{4}$$

As illustrated in Fig. 4b, the band gap energy of Bi_2MoO_6 estimated from the plot of $(\alpha h\nu)^2$ versus photo energy ($h\nu$) was 2.58 eV. The potentials of conduction band (CB) and valence band (VB) are generally determined according to the following empirical equations [46]:

$$E_{CB} = X - E_0 - \frac{1}{2}E_g \tag{5}$$

$$E_{VB} = E_{CB} + E_g \tag{6}$$

where E_{CB} is the edge potential of CB, the value of X which represents the electronegativity of the semiconductor is 5.5 eV for Bi_2MoO_6 [47], E_0 is the energy of free electrons on the hydrogen scale (about 4.5 eV), E_g is the band gap energy of the semiconductor (2.58 eV, from Eq. (4)), E_{VB} is the VB edge potential.

According to the above formulas, the E_{VB} and E_{CB} values of Bi_2MoO_6 were calculated to be 2.29 eV and − 0.29 eV, respectively.

3.2 Degradation of TC-HCl under different systems

Preliminary experiments were conducted to evaluate the degradation efficiency of TC-HCl under various systems and the results were shown in Fig. 5. No obvious degradation of TC-HCl was observed in the case of visible light irradiation, revealing that TC-HCl was quite stable under visible light. Only 4% of TC-HCl was degraded by 4 g/L PS, indicating that it was difficult for PS to directly degrade TC-HCl. Interestingly, the degradation efficiency of TC-HCl increased to 26.9% when combing visible light with 4 g/L PS. Adsorption

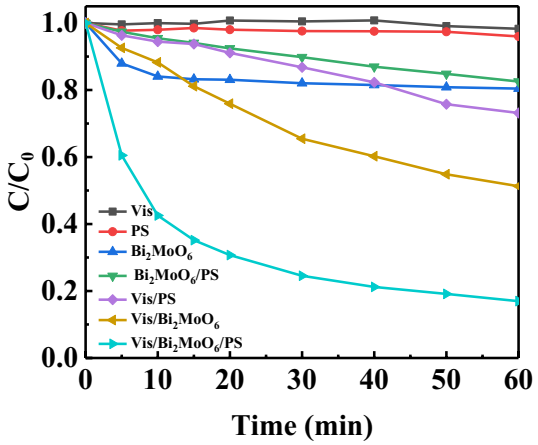

Fig. 5 Time-dependent TC-HCl concentration under different systems (conditions: Bi_2MoO_6 loading = 0.5 g/L; initial TC-HCl concentration = 20 ppm; initial PS concentration = 4 g/L; unbuffered initial pH ~ 4.4)

Table 1 The apparent rate constant (k_{app}) and correlation coefficient (R^2) for the degradation of TC at different reaction time by the Vis/Bi_2MoO_6/PS system

Time (min)	K_{app} (min^{-1})	R^2
0–60	0.0250	0.8596
0–10	0.0846	0.9923
10–60	0.0175	0.9819

capacity was investigated using bare Bi_2MoO_6 as catalyst. Approximately 20% of TC-HCl was adsorbed within 5 min but no more TC-HCl was further adsorbed. This phenomenon could be attributed to the achievement of adsorption/desorption equilibrium. Compared to PS alone, only 13% improvement of TC-HCl decay was observed in the Bi_2MoO_6/PS system, which suggested that PS was difficult to be excited by Bi_2MoO_6 in the dark. Resulting from the efficient photocatalytic activity of Bi_2MoO_6, about 48.2% of TC-HCl decay was achieved in Vis/Bi_2MoO_6 system. Compared to other systems, it was obvious that the Vis/Bi_2MoO_6/PS process exhibited the optimum performance toward TC-HCl degradation and almost 83% of TC-HCl was degraded within 60 min.

As shown in Table 1, TC-HCl degradation obeyed the two-stage pseudo first-order kinetics. The degradation process could be divided into the first (sharp) stage (t < 10 min) and the second (gradual) stage (t > 10 min). According to the previous literatures, the rate constant calculated in the first stage was commonly used to evaluate whether the combination of Vis/oxidant and Vis/catalyst was synergistic [32, 48, 49]. Table 2 presented the relative kinetic parameters for TC-HCl degradation in the first stage under various systems.

Table 2 The apparent rate constant (k_{app}) and correlation coefficient (R^2) for the degradation of TC in the first stage under different systems

Systems	Time (min)	k_{app} (min^{-1})	R^2
Vis/PS	0–10	0.0057	0.9669
Vis/Bi_2MoO_6	0–10	0.0108	0.9849
Vis/Bi_2MoO_6/PS	0–10	0.0846	0.9923

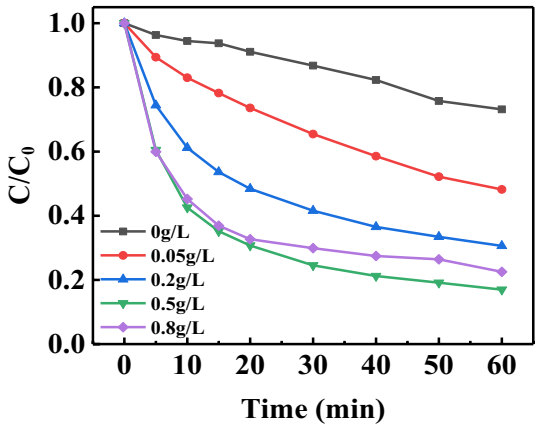

Fig. 6 Effect of Bi_2MoO_6 loading on the removal efficiency of TC-HCl with the Vis/Bi_2MoO_6/PS system (conditions: initial TC-HCl concentration = 20 ppm; initial PS concentration = 4 g/L; unbuffered initial pH ~ 4.4)

A synergy index (ratio of the degradation rate obtained with Vis/Bi_2MoO_6/PS system and the sum of degradation rates attained with Vis/PS and Vis/Bi_2MoO_6 systems) of 5.13 (≫ 1) was obtained, indicating the combination of Vis/PS and Vis/Bi_2MoO_6 was synergistic [49].

3.3 Effects of parameters on TC-HCl degradation in Vis/Bi_2MoO_6/PS system

To investigate the effect of catalyst loading on the photocatalytic degradation of TC-HCl by the Vis/Bi_2MoO_6/PS system, experiments were carried out by varying the catalyst dosages (0 to 0.8 g/L). As shown in Fig. 6, removal efficiency was markedly accelerated with an increase of catalyst loading (0 to 0.5 g/L). This phenomenon might be attributed to the increase of available active sites for PS decomposition. Nevertheless, a slight decrease of TC-HCl decay was observed with increasing the Bi_2MoO_6 loading from 0.5 to 0.8 g/L. Previous studies have reported that the existence of excessive catalyst can lead to the low rate of visible light penetration because of turbid solution caused by the formation of aggregates and consequent self-bonding of catalyst particles [32]. The catalyst dosage of 0.5 g/L with maximum

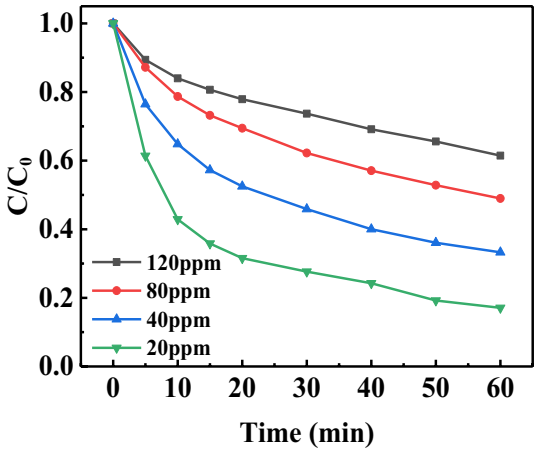

Fig. 7 Effect of TC-HCl concentration on the removal efficiency of TC-HCl with the Vis/Bi_2MoO_6/PS system (conditions: Bi_2MoO_6 loading = 0.5 g/L; initial PS concentration = 4 g/L; unbuffered initial pH ~ 4.4)

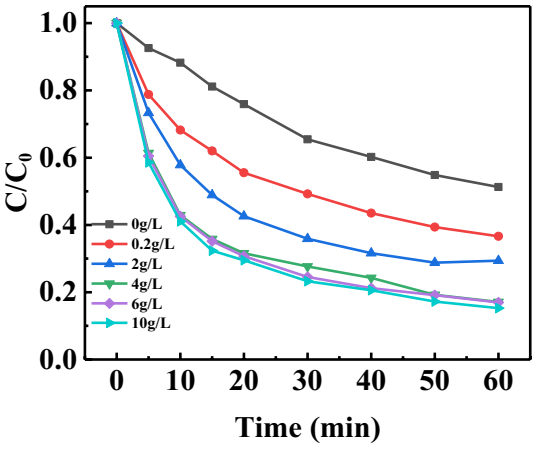

Fig. 8 Effect of PS concentration on the removal efficiency of TC-HCl with the Vis/Bi_2MoO_6/PS system (conditions: Bi_2MoO_6 loading = 0.5 g/L; initial TC-HCl concentration = 20 ppm; unbuffered initial pH ~ 4.4)

removal efficiency of TC-HCl was applied in the following experiments.

The degradation performance of Vis/Bi_2MoO_6/PS system at various initial TC-HCl concentrations was investigated and the results were presented in Fig. 7. It can be seen that the removal efficiency of TC-HCl decreased significantly with increasing the TC-HCl concentration from 20 to 120 ppm. At an initial TC-HCl concentration of 20 ppm, approximately 83% removal was achieved within 60 min. Nevertheless, the degradation rate decreased to 66.8% for 40 ppm TC-HCl, 51.1% for 80 ppm TC-HCl and 38.6% for 120 ppm TC-HCl. At high substrate concentrations, the interaction of catalyst surface and visible light was restricted because more photos would be absorbed by TC-HCl molecules or the formed by-products. Another reason might be attributed to the fact that a large number of by-products would compete with TC-HCl molecules to react with generated radicals [49].

To evaluate the influence of PS concentration on the degradation rate of TC-HCl, a series of experiments were carried out at different concentrations of PS (0 to 10 g/L). The obtained results were shown in Fig. 8. In the absence of PS, 48.2% extent of TC-HCl was removed after 60 min. The degradation rate of TC-HCl were 63.4%, 70.7%, 83% for the concentration of PS at 0.2 g/L, 2 g/L, 4 g/L, respectively. Obviously, the degradation efficiency of TC-HCl increased sharply with increasing the concentration of PS from 0 to 4 g/L. This was because more reactive radicals would generate on the surface of Bi_2MoO_6 with increasing the amount of PS which worked as the donor of sulfate and hydroxyl radicals. On the contrary, there was no promotion of degradation rate when the PS concentration further increased to 10 g/L. Excess amounts of PS could not be activated efficiently because limited active sites could be provided for PS activation at fixed Bi_2MoO_6 loading and illumination intensity. Additionally, the radical–radical recombination parasite reactions were suspected to be occurred at high concentration of radicals. Both $SO_4^{\cdot-}$ and ·OH were consumed leading to the generation of less active radicals including $S_2O_8^{\cdot-}$ and $HSO_4^{\cdot-}$ (Eqs. (7) – (10)) [50, 51]. Compared to other concentration of PS, 4 g/L which performed the quite excellent degradation efficiency was applied in the following study.

$$SO_4^{\cdot-} + S_2O_8^{2-} \rightarrow SO_4^{2-} + S_2O_8^{\cdot-} \quad (7)$$

$$SO_4^{\cdot-} + SO_4^{\cdot-} \rightarrow S_2O_8^{2-} \quad (8)$$

$$S_2O_8^{2-} + \cdot OH \rightarrow OH^- + S_2O_8^{\cdot-} \quad (9)$$

$$SO_4^{\cdot-} + \cdot OH \rightarrow HSO_4^- + 1/2O_2 \quad (10)$$

It was necessary to elucidate how initial solution pH influence the oxidation process of TC-HCl since solution pH played an important role in PS activation [34]. The solution pH was adjusted to five different pH values of 2.1, 3.4, 4.0, 6.1, 10.2 by 1 M NaOH and 1 M HNO_3. The initial solution pH without adjustment was 4.4. The results were presented in Fig. 9. The degradation of TC-HCl at three different pH values from 3.4 to 6.1 had no obvious difference from that of pH 4.4 at basic conditions. However, when the degradation process was conducted at strange acid medium (pH 2.1), the removal efficiency of TC-HCl declined rapidly with a final removal of 69.5%. This phenomenon might be due to the reaction between H^+ and active radicals (Eqs. (11) and (12)) [52]. At a pH of 10.2, the TC-HCl degradation slightly decreased to 78.8%. This decrease was attributed to the capture activity of OH^- according to Eq. (13) [53]. In

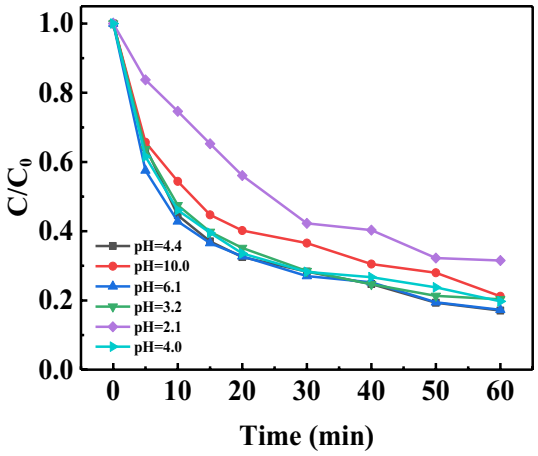

Fig. 9 Effect of solution pH on the removal efficiency of TC-HCl with the Vis/Bi_2MoO_6/PS system (conditions: Bi_2MoO_6 loading = 0.5 g/L; initial TC-HCl concentration = 20 ppm; initial PS concentration = 4 g/L)

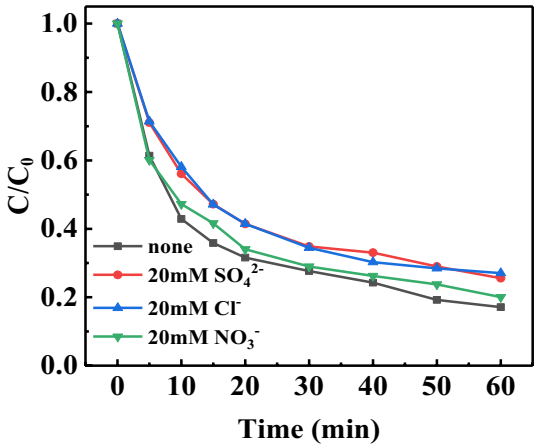

Fig. 10 Effect of coexisting anions on the removal efficiency of TC-HCl with the Vis/Bi_2MoO_6/PS system (conditions: Bi_2MoO_6 loading = 0.5 g/L; initial TC-HCl concentration = 20 ppm; initial PS concentration = 4 g/L; unbuffered initial pH ~ 4.4)

conclusion, the Vis/Bi_2MoO_6/PS system could be applied at a wide range of pH to degrade TC-HCl and the pH without adjustment is also feasible in the treatment of TC-HCl.

$$\cdot OH + H^+ + e^- \rightarrow H_2O \quad (11)$$

$$SO_4^{\cdot-} + H^+ + e^- \rightarrow HSO_4^{\bullet-} \quad (12)$$

$$SO_4^{\cdot-} + OH^- \rightarrow \cdot OH + SO_4^{2-} \quad (13)$$

In the actual water matrix, the occurrence of inorganic anions will influence the wastewater conditions even the fate of pollutants through electron exchange [53]. Figure 10 illustrated the effects of three inorganic ions including Cl^-, SO_4^{2-} and NO_3^- at a fixed concentration of 20 mM on TC-HCl degradation. Near 83% extent of TC-HCl was degraded within 60 min in the absence of anions. Nevertheless, the degradation efficiency of TC-HCl decreased to 73% in the case of 20 mM Cl^- addition. The negative effect of Cl^- resulted from the phenomenon that the existence of Cl^- will transform $SO_4^{\cdot-}$ and ·OH to selective radicals which were not favorable for TC degradation (Eqs. (14)– (16)) [54]. The presence of 20 mM SO_4^{2-} decreased the degradation efficiency of TC-HCl from 83% to 72%. The possible reactions involved in the transformation process of radicals with the addition of SO_4^{2-} were listed in Eqs. (17) and (18) [55]. A negligible influence of 20 mM NO_3^- on the degradation efficiency of TC-HCl was observed.

$$SO_4^{\cdot-} + Cl^- \rightarrow SO_4^{2-} + Cl\cdot \quad (14)$$

$$Cl^{\cdot} + Cl^- \rightarrow Cl_2^{\cdot-} \quad (15)$$

$$Cl^- + \cdot OH \rightarrow ClOH^{\cdot-} \quad (16)$$

$$^{\cdot}OH + SO_4^{2-} \rightarrow SO_4^{\cdot-} + OH^- \quad (17)$$

$$SO_4^{\cdot-} + SO_4^{2-} \rightarrow S_2O_8^{2-} + e^- \quad (18)$$

3.4 Reusability and stability of Bi_2MoO_6 in Vis/Bi_2MoO_6/PS system

Recycle experiments were carried out to investigate the reusability and stability of Bi_2MoO_6 under optimum conditions (0.5 g/L Bi_2MoO_6; 4 g/L PS; initial pH 4.4 and 20 ppm TC, from 3.3 section). After each degradation cycle, the used samples were separated immediately from TC-HCl solution by centrifugation. Subsequently, the catalyst was redispersed into fresh TC-HCl solution and the photocatalytic reactions were re-initialed under the same conditions compared to the first run. Figure 11 compared the degradation results of repeated experiments. About 83% of TC-HCl was removed within 60 min in the first run while 74.5% TC-HCl removal efficiency was achieved in the third run, which indicated that the photocatalytic efficiency of TC-HCl showed acceptable decrease even after three cycles. The recycle experiments implied that Bi_2MoO_6 was an excellent and stable catalyst in the Vis/Bi_2MoO_6/PS system.

3.5 Mechanism for TC degradation in Vis/Bi_2MoO_6/PS system

In order to detect the main reactive radicals involved in the degradation system, several quenching tests were carried out. TBA was used as the scavenger of ·OH due to its much lower rate constant with $SO_4^{\cdot-}$ (4.0×10^5 M^{-1} S^{-1})

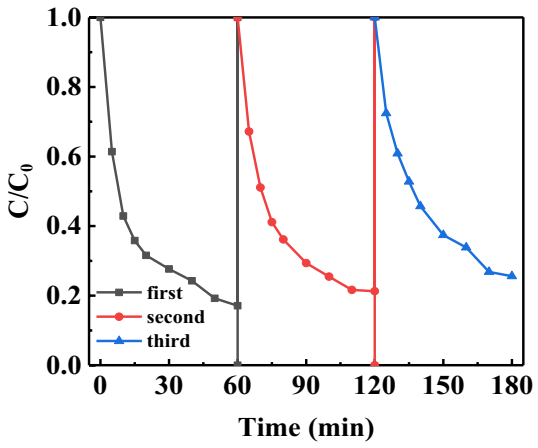

Fig. 11 Stability of Bi_2MoO_6 in Vis/Bi_2MoO_6/PS system (conditions: Bi_2MoO_6 loading = 0.5 g/L; initial TC-HCl concentration = 20 ppm; initial PS concentration = 4 g/L; unbuffered initial pH ~ 4.4)

compared to ·OH (6.0×10^8 M^{-1} S^{-1}) [56]. Phenol which reacts with $SO_4^{\cdot-}$ and ·OH at high and comparable rate constants (6.6×10^9 M^{-1} S^{-1} and 8.8×10^9 M^{-1} S^{-1} for $SO_4^{\cdot-}$ and ·OH, respectively) was employed to quench $SO_4^{\cdot-}$ and ·OH [57]. The addition of ethylenediamine tetraacetic acid disodium salt (EDTA-2Na) and Nitrogen (N_2) were applied to trap h^+ and $O_2^{\cdot-}$, respectively [58].

As illustrated in Fig. 12, when 1 mM TBA was added into the system, the degradation rate of TC-HCl decreased from 83 to 72.8%. In the presence of 1 mM phenol, the photocatalytic activity was inhibited significantly and only 35% of TC-HCl was removed after 60 min. The different inhibition effect of TBA and phenol suggested that $SO_4^{\cdot-}$ played a much more indispensable role than ·OH in the degradation process of TC-HCl [54]. The degradation efficiency of TC-HCl rapidly decreased to 11.6% with the addition of 0.5 mM EDTA-2Na, which resulted from the strong oxidization capacity of h^+ [58]. There was about 4% loss in removal efficiency of TC under N_2 saturation, indicating that $O_2^{\cdot-}$ also participated in the degradation process but played a negligible role.

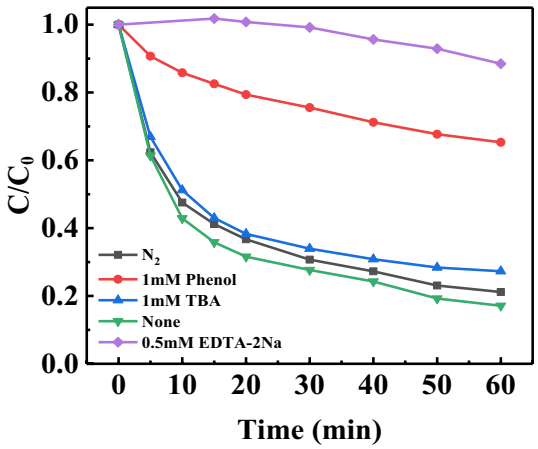

Fig. 12 Effect of radical scavengers on the removal efficiency of TC-HCl with the Vis/Bi_2MoO_6/PS system (conditions: Bi_2MoO_6 loading = 0.5 g/L; initial TC-HCl concentration = 20 ppm; initial PS concentration = 4 g/L; unbuffered initial pH ~ 4.4)

According to these trapping experiments, a possible mechanism was proposed to explain the enhanced photocatalytic performance toward the degradation of TC-HCl by Vis/Bi_2MoO_6/PS system. As shown in Fig. 13, under visible light illumination, the catalyst was excited with the generation of electron–hole pairs (Eq. (19)). PS activation was achieved by the reaction between free electrons on the conduction band and PS anions (Eq. (20)) [34]. As electrons were partly consumed by PS, the recombination rate of photo-induced electron/hole pairs was decelerated. Furthermore, $SO_4^{\cdot-}$ would react with H_2O/OH^- resulting in the production of ·OH (Eqs. (21)– (22)) [59]. ·OH cannot be generated through sole photocatalysis since the potential of h^+ on the valence band of Bi_2MoO_6 (2.29 eV) was more negative than the potential of $H_2O/{\cdot}OH$ (2.4 eV) [26]. The dissolved oxygen (O_2) was difficult to be reduced by the photo-induced e^- to $O_2^{\cdot-}$ because the reduction potential of conduction band for Bi_2MoO_6 (− 0.29 eV) was a little lower than the potential of $O_2/O_2^{\cdot-}$ (− 0.33 eV) [60]. h^+ on the conduction band could directly react with organic compounds [26].

$$Bi_2MoO_6 + h\nu \rightarrow h^+ + e^- \quad (19)$$

$$S_2O_8^{2-} + e^- \rightarrow SO_4^{\cdot-} + SO_4^{2-} \quad (20)$$

$$SO_4^{\cdot-} + H_2O \rightarrow {\cdot}OH + SO_4^{2-} + H^+ \quad (21)$$

$$SO_4^{\cdot-} + OH^- \rightarrow {\cdot}OH + SO_4^{2-} \quad (22)$$

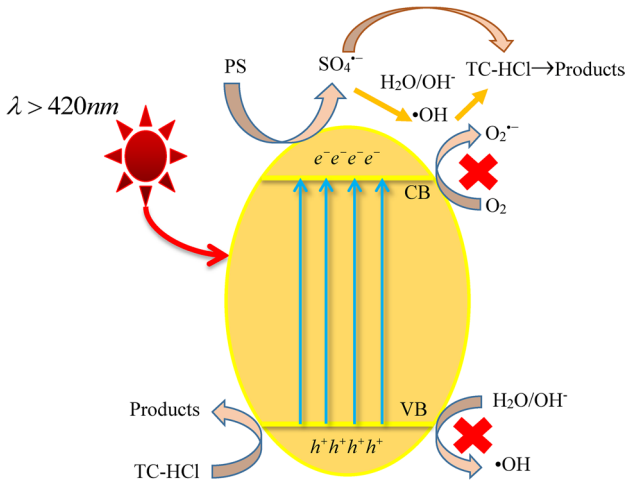

Fig. 13 The schematic diagram of Vis/Bi_2MoO_6/PS phtotocatalytic system

$$SO_4^{\cdot-}/{}^{\cdot}OH/h^+ + TC - HCl \rightarrow products \quad (23)$$

4 Conclusions

In our study, the ternary Vis/Bi_2MoO_6/PS system was proved to be more efficient than unary or binary systems toward TC-HCl removal in aqueous phase. Increasing Bi_2MoO_6 dosage or PS concentration in a range would rapidly accelerate the degradation process. Higher TC-HCl concentrations were adverse to the process of TC-HCl removal. The novel system demonstrated ideal removal efficiency at a wide range of initial solution pH. The existence of inorganic anions such as Cl^- and SO_4^{2-} had a negative effect on the TC-HCl removal efficiency while NO_3^- did not affect it. The catalyst exhibited excellent reusability and stability in multiple runs. The results of trapping experiments indicated that $SO_4^{\cdot-}$ together with h^+ were mainly responsible for the degradation process. A suitable mechanism was proposed to explain the rate-enhancing effect of Vis/Bi_2MoO_6/PS system. After the catalyst was activated by visible light, PS would react with e^- which resulted in the generation of $SO_4^{\cdot-}$ and ·OH. Meanwhile, the recombination rate of electron/hole pairs was decelerated since part of e^- was consumed by PS. In summary, degrading organic pollutants using Vis/Bi_2MoO_6/PS system is a promising technology.

Acknowledgements This work was supported by the National Natural Science Foundation of China (No. 21277108).

References

1. F. Deng, L. Zhao, X. Luo, S. Luo, D.D. Dionysiou, Highly efficient visible-light photocatalytic performance of Ag/$AgIn_5S_8$ for degradation of tetracycline hydrochloride and treatment of real pharmaceutical industry wastewater. Chem. Eng. J. **333**, 423–433 (2018)
2. C. Li, S. Yu, H. Dong, Y. Wang, H. Wu, X. Zhang, G. Chen, C. Liu, Mesoporous ferriferrous oxide nanoreactors modified on graphitic carbon nitride towards improvement of physical, photoelectrochemical properties and photocatalytic performance. J. Colloid Interface Sci. **531**, 331–342 (2018)
3. C. Li, S. Yu, X. Zhang, Y. Wang, C. Liu, G. Chen, H. Dong, Insight into photocatalytic activity, universality and mechanism of copper/chlorine surface dual-doped graphitic carbon nitride for degrading various organic pollutants in water. J. Colloid Interface Sci. **538**, 462–473 (2019)
4. S. Ma, J. Xue, Y. Zhou, Z. Zhang, Enhanced visible-light photocatalytic activity of Ag_2O/g-C_3N_4 p-n heterojunctions synthesized via a photochemical route for degradation of tetracycline hydrochloride. RSC Adv. **5**, 40000–40006 (2015)
5. J. Qin, L. Xie, Y. Ying, Determination of tetracycline hydrochloride by terahertz spectroscopy with PLSR model. Food Chem. **170**, 415–422 (2015)
6. C. Peiris, S.R. Gunatilake, T.E. Mlsna, D. Mohan, M. Vithanage, Biochar based removal of antibiotic sulfonamides and tetracyclines in aquatic environments: a critical review. Bioresour. Technol. **246**, 150–159 (2017)
7. Q. Liu, L. Zhong, Q. Zhao, C. Frear, Y.M. Zheng, Synthesis of Fe_3O_4/polyacrylonitrile composite electrospun nanofiber mat for effective adsorption of tetracycline. ACS Appl. Mater. Interfaces **7**, 14573–14583 (2015)
8. H. Wang, Y. Wu, M. Feng, W. Tu, T. Xiao, T. Xiong, H. Ang, X. Yuan, J.W. Chew, Visible-light-driven removal of tetracycline antibiotics and reclamation of hydrogen energy from natural water matrices and wastewater by polymeric carbon nitride foam. Water Res. **144**, 215–225 (2018)
9. J. Xue, S. Ma, Y. Zhou, Z. Zhang, M. He, Facile photochemical synthesis of Au/Pt/g-C_3N_4 with plasmon-enhanced photocatalytic activity for antibiotic degradation. ACS Appl. Mater. Interfaces **7**, 9630–9637 (2015)
10. B. Yin, Z. Fang, B. Luo, G. Zhang, W. Shi, Facile preparation of $Bi_{24}O_{31}Cl_{10}$ nanosheets for visible-light-driven photocatalytic degradation of tetracycline hydrochloride. Catal. Lett. **147**, 2167–2172 (2017)
11. W. Wang, K. Xiao, L. Zhu, Y. Yin, Z. Wang, Graphene oxide supported titanium dioxide & ferroferric oxide hybrid, a magnetically separable photocatalyst with enhanced photocatalytic activity for tetracycline hydrochloride degradation. RSC Adv. **7**, 21287–21297 (2017)
12. K. Yang, Q. Yue, J. Kong, P. Zhao, Y. Gao, K. Fu, B. Gao, Microbial diversity in combined UAF–UBAF system with novel sludge and coal cinder ceramic fillers for tetracycline wastewater treatment. Chem. Eng. J. **285**, 319–330 (2016)
13. F. Deng, F. Zhong, D. Lin, L. Zhao, Y. Liu, J. Huang, X. Luo, S. Luo, D.D. Dionysiou, One-step hydrothermal fabrication of visible-light-responsive $AgInS_2$/$SnIn_4S_8$ heterojunction for highly-efficient photocatalytic treatment of organic pollutants and real pharmaceutical industry wastewater. Appl. Catal. B **219**, 163–172 (2017)
14. Y. Hong, C. Li, G. Zhang, Y. Meng, B. Yin, Y. Zhao, W. Shi, Efficient and stable Nb_2O_5 modified g-C_3N_4 photocatalyst for removal of antibiotic pollutant. Chem. Eng. J. **299**, 74–84 (2016)
15. Y. Zhang, J. Zhou, X. Chen, Q. Feng, W. Cai, MOF-derived C-doped ZnO composites for enhanced photocatalytic performance under visible light. J. Alloys Compd. **777**, 109–118 (2019)
16. W. Liu, J. Zhou, Z. Hu, J. Zhou, W. Cai, In situ facile fabrication of Z-scheme leaf-like beta-Bi_2O_3/g-C_3N_4 nanosheets composites with enhanced visible light photoactivity. J. Mater. Sci. Mater. Electron. **29**, 14906–14917 (2018)
17. Z. Hu, J. Zhou, Y. Zhang, W. Liu, J. Zhou, W.Q. Cai, The formation of a direct Z-scheme Bi_2O_3/MoO_3 composite nanocatalyst with improved photocatalytic activity under visible light. Chem. Phys. Lett. **706**, 208–214 (2018)
18. W. Liu, J. Zhou, J. Zhou, Facile fabrication of multi-walled carbon nanotubes (MWCNTs)/α-Bi_2O_3 nanosheets composite with enhanced photocatalytic activity for doxycycline degradation under visible light irradiation. J. Mater. Sci. **54**, 3294–3308 (2018)
19. J. Ding, Z.Q. Yang, C. He, X.W. Tong, Y. Li, X.J. Niu, H.G. Zhang, UiO-66(Zr) coupled with Bi_2MoO_6 as photocatalyst for visible-light promoted dye degradation. J. Colloid Interface Sci. **497**, 126–133 (2017)
20. A. Rauf, M. Shah, G.H. Choi, U.B. Humayoun, D.H. Yoon, J.W. Bae, J. Park, W.J. Kim, P.J. Yoo, Facile synthesis of hierarchically structured Bi_2S_3/Bi_2WO_6 photocatalysts for highly efficient reduction of Cr(VI). ACS Sustain. Chem. Eng. **3**, 2847–2855 (2015)
21. X. Gao, C. Ma, Y. Liu, L. Xing, Y. Yan, Self-induced Fenton reaction constructed by Fe(III) grafted $BiVO_4$ nanosheets with improved photocatalytic performance and mechanism insight. Appl. Surf. Sci. **467–468**, 673–683 (2019)
22. X. Li, W. Zhang, W. Cui, J. Li, Y. Sun, G. Jiang, H. Huang, Y. Zhang, F. Dong, Reactant activation and photocatalysis

mechanisms on Bi-metal@Bi_2GeO_5 with oxygen vacancies: a combined experimental and theoretical investigation. Chem. Eng. J. **370**, 1366–1375 (2019)
23. J. Zhou, J. Zhou, Z. Hu, L. Wang, Enhancement of adsorption and visible light photocatalytic activity of the Zn^{2+}-doped BiOBr/PVP modified microspheres for RhB. Mater. Sci. Semicond. Process. **90**, 112–119 (2019)
24. X. Dong, W. Cui, H. Wang, J. Li, Y. Sun, H. Wang, Y. Zhang, H. Huang, F. Dong, Promoting ring-opening efficiency for suppressing toxic intermediates during photocatalytic toluene degradation via surface oxygen vacancies. Sci. Bull. **64**, 669–678 (2019)
25. J. Li, X. Dong, G. Zhang, W. Cui, W. Cen, Z. Wu, S.C. Lee, F. Dong, Probing ring-opening pathways for efficient photocatalytic toluene decomposition. J. Mater. Chem. A **7**, 3366–3374 (2019)
26. T.P. Hu, Y. Yang, K. Dai, J.F. Zhang, C.H. Liang, A novel Z-scheme Bi_2MoO_6/BiOBr photocatalyst for enhanced photocatalytic activity under visible light irradiation. Appl. Surf. Sci. **456**, 473–481 (2018)
27. L. Yan, Y.F. Wang, H.D. Shen, Y. Zhang, J. Li, D.J. Wang, Photocatalytic activity of Bi_2WO_6/Bi_2S_3 heterojunctions: the facilitation of exposed facets of Bi_2WO_6 substrate. Appl. Surf. Sci. **393**, 496–503 (2017)
28. Y.L. Jia, Y.H. Lin, Y. Ma, W.B. Shi, Fabrication of hollow Bi_2MoO_6 nanorods with efficient photocatalytic performance. Mater. Lett. **234**, 83–86 (2019)
29. D.P. Dutta, A. Ballal, S. Chopade, A. Kumar, A study on the effect of transition metal (Ti^{4+}, Mn^{2+}, Cu^{2+} and Zn^{2+})-doping on visible light photocatalytic activity of Bi_2MoO_6 nanorods. J. Photochem. Photobiol. A **346**, 105–112 (2017)
30. J.L. Lv, J.F. Zhang, J. Liu, Z. Li, K. Dai, C.H. Liang, Bi SPR-promoted Z-scheme Bi_2MoO_6/CdS-diethylenetriamine composite with effectively enhanced visible light photocatalytic hydrogen evolution activity and stability. ACS Sustain. Chem. Eng. **6**, 696–706 (2018)
31. W.L. Dai, X. Hu, T.Y. Wang, W.W. Xiong, X.B. Luo, J.P. Zou, Hierarchical CeO_2/Bi_2MoO_6 heterostructured nanocomposites for photoreduction of CO_2 into hydrocarbons under visible light irradiation. Appl. Surf. Sci. **434**, 481–491 (2018)
32. A.T. Nguyen, R.S. Juang, Photocatalytic degradation of p-chlorophenol by hybrid H_2O_2 and TiO_2 in aqueous suspensions under UV irradiation. J. Environ. Manag. **147**, 271–277 (2015)
33. M. Brienza, M.M. Ahmed, A. Escande, G. Plantard, L. Scrano, S. Chiron, S.A. Bufo, V. Goetz, Relevance of a photo-Fenton like technology based on peroxymonosulphate for 17 beta-estradiol removal from wastewater. Chem. Eng. J. **257**, 191–199 (2014)
34. Y. Zhang, J. Zhou, X. Chen, L. Wang, W. Cai, Coupling of heterogeneous advanced oxidation processes and photocatalysis in efficient degradation of tetracycline hydrochloride by Fe-based MOFs: synergistic effect and degradation pathway. Chem. Eng. J. **369**, 745–757 (2019)
35. Y. Jo, C. Kim, G.-H. Moon, J. Lee, T. An, W. Choi, Activation of peroxymonosulfate on visible light irradiated TiO_2 via a charge transfer complex path. Chem. Eng. J. **346**, 249–257 (2018)
36. Y. Gong, B. Yang, H. Zhang, X. Zhao, A g-C_3N_4/MIL-101(Fe) heterostructure composite for highly efficient BPA degradation with persulfate under visible light irradiation. J. Mater. Chem. A **6**, 23703–23711 (2018)
37. K.B. Dhanalakshmi, S. Anandan, J. Madhavan, P. Maruthamuthu, Photocatalytic degradation of phenol over TiO_2 powder: the influence of peroxomonosulphate and peroxodisulphate on the reaction rate. Sol. Energy Mater. Sol. Cells **92**, 457–463 (2008)
38. Y. Shi, H. Chen, Y. Wu, W. Dong, Degradation of atenolol via heterogeneous activation of persulfate by using BiOCl@Fe_3O_4 catalyst under simulated solar light irradiation. Environ. Sci. Pollut. Res. Int. **25**, 693–703 (2018)
39. Y. Zhou, Y. Zhang, M. Lin, J. Long, Z. Zhang, H. Lin, J.C. Wu, X. Wang, Monolayered Bi_2WO_6 nanosheets mimicking heterojunction interface with open surfaces for photocatalysis. Nat. Commun. **6**, 8340 (2015)
40. K.Q. Jing, J.H. Xiong, N. Qin, Y.J. Song, L.Y. Li, Y. Yu, S.J. Liang, L. Wu, Development and photocatalytic mechanism of monolayer Bi_2MoO_6 nanosheets for the selective oxidation of benzylic alcohols. Chem. Commun. **53**, 8604–8607 (2017)
41. Y.H. Ma, F. Chen, Q. Yang, Y. Zhong, X.Y. Shu, F.B. Yao, T. Xie, X.M. Li, D.B. Wang, G.M. Zeng, Sulfate radical induced degradation of Methyl Violet azo dye with CuFe layered doubled hydroxide as heterogeneous photoactivator of persulfate. J. Environ. Manag. **227**, 406–414 (2018)
42. C.L. Yu, Z. Wu, R.Y. Liu, D.D. Dionysiou, K. Yang, C.Y. Wang, H. Liu, Novel fluorinated Bi_2MoO_6 nanocrystals for efficient photocatalytic removal of water organic pollutants under different light source illumination. Appl. Catal. B **209**, 1–11 (2017)
43. Y.X. Xing, X.C. Gao, G.F. Ji, Z.L. Liu, C.F. Du, Synthesis of carbon doped Bi_2MoO_6 for enhanced photocatalytic performance and tumor photodynamic therapy efficiency. Appl. Surf. Sci. **465**, 369–382 (2019)
44. P. Zhang, X.X. Teng, G.Q. Zhang, D.S. Liu, L. Fu, H.L. Xie, S.M. Ding, Facile Br-assisted hydrothermal synthesis of Bi_2MoO_6 nanoplates with enhanced visible-light photocatalytic activity. Appl. Phys. A **123**, 632 (2017)
45. Y. Bian, W.X. Zeng, M. He, Y.J. Ma, Y. Liu, Y. Kong, J. Pan, Boosting charge transfer via molybdenum doping and electric-field effect in bismuth tungstate: density function theory calculation and potential applications. J. Colloid Interface Sci. **534**, 20–30 (2019)
46. J. Li, W. Guan, X. Yan, Z. Wu, W. Shi, Photocatalytic ozonation of 2,4-dichlorophenoxyacetic acid using $LaFeO_3$ photocatalyst under visible light irradiation. Catal. Lett. **148**, 23–29 (2017)
47. J. Zhang, L. Zhang, N. Yu, K. Xu, S. Li, H. Wang, J. Liu, Flower-like Bi_2S_3/Bi_2MoO_6 heterojunction superstructures with enhanced visible-light-driven photocatalytic activity. RSC Adv. **5**, 75081–75088 (2015)
48. A.T. Nguyen, C.T. Hsieh, R.S. Juang, Substituent effects on photodegradation of phenols in binary mixtures by hybrid H_2O_2 and TiO_2 suspensions under UV irradiation. J. Taiwan Inst. Chem. Eng. **62**, 68–75 (2016)
49. S. Bekkouche, S. Merouani, O. Hamdaoui, M. Bouhelassa, Efficient photocatalytic degradation of Safranin O by integrating solar-UV/TiO_2/persulfate treatment: implication of sulfate radical in the oxidation process and effect of various water matrix components. J. Photochem. Photobiol. A **345**, 80–91 (2017)
50. Y. Gao, S. Li, Y. Li, L. Yao, H. Zhang, Accelerated photocatalytic degradation of organic pollutant over metal-organic framework MIL-53(Fe) under visible LED light mediated by persulfate. Appl. Catal. B **202**, 165–174 (2017)
51. H. Ferkous, S. Merouani, O. Hamdaoui, C. Petrier, Persulfate-enhanced sonochemical degradation of naphthol blue black in water: evidence of sulfate radical formation. Ultrason. Sonochem. **34**, 580–587 (2017)
52. A. Abdelhaleem, W. Chu, Monuron photodegradation using peroxymonosulfate activated by non-metal-doped TiO_2 under visible LED and the modeling via a parallel-serial kinetic approach. Chem. Eng. J. **338**, 411–421 (2018)
53. L.W. Chen, D.H. Ding, C. Liu, H. Cai, Y. Qu, S.J. Yang, Y. Gao, T.M. Cai, Degradation of norfloxacin by $CoFe_2O_4$-GO composite coupled with peroxymonosulfate: a comparative study and mechanistic consideration. Chem. Eng. J. **334**, 273–284 (2018)
54. J. Deng, M.Y. Xu, C.G. Qiu, Y. Chen, X.Y. Ma, N.Y. Gao, X.Y. Li, Magnetic $MnFe_2O_4$ activated peroxymonosulfate processes for degradation of bisphenol A: performance, mechanism and application feasibility. Appl. Surf. Sci. **459**, 138–147 (2018)

55. M. Sayed, J.A. Khan, L.A. Shah, N.S. Shah, F. Shah, H.M. Khan, P. Zhang, H. Arandiyan, Solar light responsive poly(vinyl alcohol)-assisted hydrothermal synthesis of immobilized TiO_2/Ti film with the addition of peroxymonosulfate for photocatalytic degradation of ciprofloxacin in aqueous media: a mechanistic approach. J. Phys. Chem. C **122**, 406–421 (2018)
56. Y. Feng, C.Z. Liao, L.J. Kong, D.L. Wu, Y.M. Liu, P.H. Lee, K. Shih, Facile synthesis of highly reactive and stable Fe-doped g-C_3N_4 composites for peroxymonosulfate activation: a novel non-radical oxidation process. J. Hazard. Mater. **354**, 63–71 (2018)
57. Q.F. Wang, Y.S. Shao, N.Y. Gao, W.H. Chu, J.X. Chen, X. Lu, Y.P. Zhu, N. An, Activation of peroxymonosulfate by Al_2O_3-based $CoFe_2O_4$ for the degradation of sulfachloropyridazine sodium: kinetics and mechanism. Sep. Purif. Technol. **189**, 176–185 (2017)
58. F. Chen, Q. Yang, D.B. Wang, F.B. Yao, Y.H. Ma, X.M. Li, J.J. Wang, L.H. Jiang, L.L. Wang, H.Q. Yu, Highly-efficient degradation of amiloride by sulfate radicals-based photocatalytic processes: reactive kinetics, degradation products and mechanism. Chem. Eng. J. **354**, 983–994 (2018)
59. S. Jorfi, B. Kakavandi, H.R. Motlagh, M. Ahmadi, N. Jaafarzadeh, A novel combination of oxidative degradation for benzotriazole removal using TiO_2 loaded on ($FeFe_2O_4$)-Fe-II-O-III@C as an efficient activator of peroxymonosulfate. Appl. Catal. B **219**, 216–230 (2017)
60. L.H. Ai, C.H. Zhang, L.L. Li, J. Jiang, Iron terephthalate metal-organic framework: revealing the effective activation of hydrogen peroxide for the degradation of organic dye under visible light irradiation. Appl. Catal. B **148**, 191–200 (2014)